Marine and Petroleum Geology 45 (2013) 198–207

Contents lists available at SciVerse ScienceDirect

Marine and Petroleum Geology

journal homepage: www.elsevier.com/locate/marpetgeo

# The stability of gas hydrate field in the northeastern continental slope of Sakhalin Island, Sea of Okhotsk, as inferred from analysis of heat flow data and its implications for slope failures

Young-Gyun Kim*, Sang-Mook Lee, Young Keun Jin, Boris Baranov, Anatoly Obzhirov, Alexander Salomatin, Hitoshi Shoji

*Korea Polar Research Institute, Division of Polar Earth-System Sciences, 26, Songdomirae-ro, Yeonsu-gu, Incheon 406-840, Republic of Korea*

ARTICLE INFO

*Article history:*
Received 11 May 2012
Received in revised form
2 April 2013
Accepted 5 May 2013
Available online 17 May 2013

*Keywords:*
Gas hydrate stability zone
Slope failure
Background heat flow
Sakhalin continental slope
Okhotsk Sea

ABSTRACT

The sudden release of methane from seas due to ocean warming and/or sea level drop, leading to extensive mass wasting at continental margins, has been suggested as a possible cause of global climate change. In the northeastern continental slope of the Sakhalin Island (Sea of Okhotsk), numerous gas hydrate-related manifestations have been reported, including hydroacoustic anomaly (gas flare) in the water column, pockmarks and mounds on the seafloor, seepage structures and bottom-simulating reflectors (BSRs). The gas hydrate found at 385 mbsl represents the shallowest occurrence ever recorded in the Okhotsk Sea. In this study, we modeled the gas hydrate stability zone (GHSZ) using methane gas composition, water temperature and geothermal gradient to see if it is consistent with the observed depth of the BSR. An important distinction can be made between the seafloor containing seepage features and normal seafloor in terms of their thermal structure. The depth of the BSR matches well with the base of GHSZ estimated from the background heat flow (geothermal gradient). A large slope failure feature is found in the northern Sakhalin continental slope. We explore the possibility that this failure was caused by gas hydrate dissociation, based on the past climate change history and inference from the GHSZ calculation. Prediction of the natural landslide is difficult; however, new stratigraphic evidence from subbottom profiles suggests that the landslide occurred at 20 ka which is roughly consistent with the late stage of the Last Glacial Maximum.



## 1. Introduction

Gas hydrate is a gas clathrate consisting of water and gas molecules, commonly found in the modern-day seafloors in deep water (e.g., Matsumoto et al., 2011). Because it is stable under high pressure and cold temperature conditions, gas hydrate is frequently found in polar regions, below onshore permafrost and in arctic oceans, and in superficial section of marine sediments of continental margins (Kvenvolden, 1998). Gas hydrate has been suggested as a source of energy (Collett, 2002) and potential geohazard including mass wasting and ensuing tsunami (Bouriak et al., 2000; Paull et al., 2000), and as a factor affecting global climate change if a large amount of greenhouse gas is suddenly released into the atmosphere (Kennett et al., 2000).

Since the first finding of methane hydrate in the Okhotsk Sea in 1986 (Zonenshayn et al., 1987), numerous geophysical surveys have been carried out in this region by KOMEX (Kurile-Okhotsk sea Marine EXperiment) (Lüdmann and Wong, 2003; Obzhirov et al., 2004; Wong et al., 2003), and more recently, by CHAOS (hydroCarbon Hydrate Accumulation in the Okhotsk Sea) and SSGH (Sakhalin Slope Gas Hydrate) projects. While the KOMEX project tried to elucidate the overall geologic features of the western Okhotsk Sea, the CHAOS and SSGH projects, have examined the detailed aspects of gas hydrate system in the northeastern continental slope of Sakhalin Island (Hachikubo et al., 2009; Jin et al., 2011; Shoji et al., 2005).

The northeastern continental slope of Sakhalin Island is also well known for its diverse manifestations of gas hydrate (Jin et al., 2011; Obzhirov et al., 2004; Shoji et al., 2005). A widespread occurrence of bottom-simulating reflectors and numerous seepage structures as well as pockmarks and mounds can be seen on the seafloor. Gas flares can also be frequently observed from echosounders. In this region, gas hydrate was recovered at a depth as shallow as 385 mbsl due to the cold water temperature, comparable to arctic regions (e.g., Biastoch et al., 2011). However, the

* Corresponding author. Tel.: +82 32 760 5459.
*E-mail address:* ygkim@kopri.re.kr (Y.-G. Kim).

0264-8172/$ – see front matter © 2013 Elsevier Ltd. All rights reserved.
http://dx.doi.org/10.1016/j.marpetgeo.2013.05.003

spatial and temporal relationships among various gas-hydrate-related features are not well understood.

Understanding the extent of the gas hydrate stability zone (GHSZ) in this region would provide an important constraint in explaining the relationships among diverse features and their possible variations. Theoretically, the stability of gas hydrate depends on numerous factors including pressure and temperature, salinity (de Roo et al., 1983), gas composition (Sloan, 1990), gas concentrations in the pore water (Xu and Ruppel, 1999), dissolved ion contents (Dickens and Quinby-Hunt, 1997), pore size (Turner et al., 2005) and mineralogy of host sediment (Cha et al., 1988) to name a few. However, the factors affecting the GHSZ may be divided conceptually into regional and local factors. By considering that the effects of local factors can be averaged out over a wide region or assuming that they are pertinent to special features or phenomena, one may simplify the relationship. Of course, the validity of such an approximation or model needs to be checked. One of the goals of this study is to compare regional parameters with observed manifestations of gas hydrates. In particular, we investigate the role of background heat flow (geothermal gradient) on the stability of gas hydrate zone.

One of the important features in our study area is the evidence for massive landslide in the northern slope. If the landslide was really caused by gas hydrate dissociation, it would represent a rare modern-day example. Previously Wong et al. (2003) argued that this slide event occurred before 350 ka. However, a careful reexamination of subbottom profiler data together with reassessment on the sedimentation rate sheds a new light on the timing of this landslide.

## 2. Environmental setting

The Sea of Okhotsk is a marginal sea of the Northwest Pacific, semi-enclosed to the east by the Kamchatka Peninsula, to the west by the Sakhalin Island, and to the south by the Kuril Islands. The straits along the Kuril Islands serve as pathways for exchange of sea waters between the Okhotsk Sea and the Pacific. According to Kitani (1973) and Talley and Nagata (1995), the surface water flows inward along the west of Kamchatka Peninsula and outward along the east of Sakhalin Island, thus making a counterclockwise rotation before exiting to the Northwest Pacific.

Sea-ice forms during the winter as a result of an influx of fresh water from the Amur River and westerly cold winds (Katsuki et al., 2010). The formation of ice has a strong influence on the water temperature profile in this region especially at shallow depth. A subzero minimum-temperature (as low as −1.7 °C) develops at a depth of 50–150 mbsl by influx of cold water from melted ice. In the summer, the water temperature at shallow depth is largely affected by the halocline (Gorbarenko et al., 2002a). However, the water temperature stays almost constant (2.5–3 °C) below 800 mbsl.

Geologically, the Sea of Okhotsk is bounded by the North American, Eurasian, Amurian, and Pacific plates (Fig. 1a). Most of the large earthquakes in the Sea of Okhotsk are caused by the subduction of the Pacific plate and are located along the Kuril Island arc. In addition, many small earthquakes were recorded in the regions far away from the trench including the Sakhalin Shear Zone which runs N–S along the Sakhalin Island.

The Sea of Okhotsk can roughly be divided into two regions: a broad continental shelf/slope to the north with water depth less

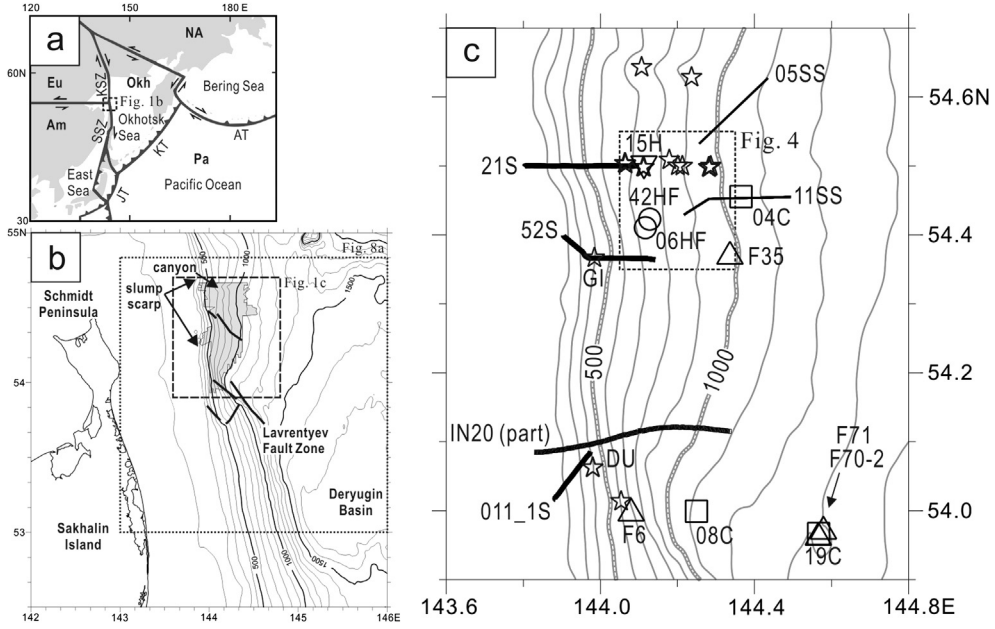


**Figure 1.** The location of the study area in the northern slope of Sakhalin slope, Sea of Okhotsk. (a) The Okhotsk plate (*Okh*) is bounded by 4 tectonic plates: North America (*NA*), Eurasia (*EU*), Amurian (*Am*), and Pacific (*Pa*) plates. Kashevarov Shear Zone (*KSZ*) and Sakhalin Shear Zone (*SSZ*) exhibit dextral movement. *JT* = Japan Trench, *KT* = Kuril Trench, *AT* = Aleutian Trench. The *box* represents the location of Figure 1b. (b) The study area, presented as *box*, is located in the northeastern continental slope of Sakhalin Island. The Deryugin Basin lies to the west. The *thick lines* indicate major faults in this region. *Lavrentyev Fault Zone* in the southern part of the study area divides cross-section slope morphology into 2 types: concave-upward to the north of itself, and convex-upward to the south (see text and Fig. 8). The *shaded area* represents the coverage of side-scan sonar survey. The *boxes* represent the location of Figures 1c and 8a, respectively. (c) The detailed map of survey area. The seismic survey lines (*thick lines*) conducted using the sparker instrument, the subbottom survey line (*thin line*), the locations of CTD casting sites to measure water temperature and salinity (*squares*), gas flare detected by hydroacoustic survey (*triangles*), and heat flow measurements (*circles*) are shown. The *reverse triangle* represents a site where core containing the gas hydrate was retrieved (see text). The bathymetric contour is shown at 100-m interval. Sites where sediment cores containing gas hydrates were taken are shown in *star* symbols: *DU* = Dungeon and *GI* = Giselle structure. The *box* represents the location of Figure 4.

than 1500 m and a deeper section to the south, which generally correspond to the Kuril Basin, formed by back-arc spreading associated with strike-slip along the SSZ (Baranov et al., 2002). Within the broad continental slope the Deryugin Basin lies to the east of our study area (Fig. 1b and c). The maximum water depth in this basin is ~1760 mbsl. According to Rodnikov et al. (2002), sediment thickness in the basin can reach up to 12 km. They also argued that a hot mantle plume is present in this basin. Although its extent and timing is not clear at this stage, high heat flow (>120 mW/m$^2$) was found only in the basin center (Tanaka et al., 2004).

An Early Oligocene-to-recent sedimentary succession with 9–14 km in thickness is observed in the study area as a result of sediment outflow from the paleo-Amur River (Kharakhinov, 1998, 2010). The exact thickness of the succession and the nature of the underlying acoustic basement are presently not clear. According to Worrall et al. (1996), the abundance of gas within sediments may be one of the important factors obscuring the seismic image.

An important morphological feature in this area is that the profile of the slope is very different between the north and south of the Lavrentyev Fault Zone (LFZ): it is concave-upward in the northern part and convex-upward in the southern part (Fig. 1b). Based on sedimentary core analysis, Wong et al. (2003) insist that such a difference in morphology is caused by mass wasting in the northern part and its timing is not later than 350 ka.

During the Quaternary, a unique oceanographic current pattern is thought to have developed in the region, resulting for instance in widespread deposition by bottom currents (contourites, sediment waves) in the Northern Sakhalin slope, and erosion and sediment reworking on the Northern Sakhalin shelf (Wong et al., 2003). In addition, mass-wasting deposits were found, which might have been triggered by shallow earthquakes or by slope failure associated with gas hydrate dissociation. The high rate of sediment outflow near the mouth of the Amur River together with high content of organic carbon within the sediment (Astakhov et al., 1998; Gorbarenko and Nürnberg, 2002b) makes this region a favorable location for gas generation and accumulation.

## 3. Survey data

Most of the data used in this study were collected during marine surveys as part of the CHAOS (2003, 2005, 2006) and SSGH (2007, 2008, 2009) projects. The latter is still on-going and will continue till 2015. One of the areas CHAOS and SSGH projects focused on is the northeastern continental slope of Sakhalin Island. A large amount of geophysical, geochemical, oceanographic, biological, and sedimentological data were obtained using the Russian research vessel *Akademik M. A. Lavrentyev* (Jin et al., 2007, 2008; Matveeva et al., 2005; Mazurenko, 2006; Shoji et al., 2008, 2010). Isotope analyses on pore water within sediments and gas hydrate samples were also performed. The gas hydrates in this area mostly consist of biogenic methane (>97.8%) with minor amount of thermogenic hydrocarbon gases (Hachikubo et al., 2009).

The presence of gas in the northeastern continental slope of Sakhalin Island can be recognized through diverse forms and structures that were created as a consequence. The manifestations include gas flares within the water column, seepages, mounds and pockmarks on the seafloor, actual gas hydrate, and BSR and chimney-like structures within the sediment.

During the CHAOS project (Jin et al., 2007; Matveeva et al., 2005; Mazurenko, 2006), 51 sparker seismic lines over ~1100 km and side-scan sonar image of ~650 km$^2$ were obtained as well as conductivity, temperature and depth sensor (CTD) profiles at 63 stations and sediment cores at 69 stations. The geothermal gradient was also measured at 8 stations. In total, over 500 gas flares and over 40 seepage structures were found.

Based on preliminary findings obtained from the CHAOS project, detailed investigations and full-coverage mapping studies at particular sites were conducted during the SSGH project. In 2007, 2008, side-scan sonar image of total ~2000 km$^2$ at three areas and 52 subbottom profile lines of ~1270 km were collected. About 130 new gas flares were recognized. In 2009, sediment coring and CTD water sampling were made around the seepage structures. Twenty one sediment cores and 11 CTD profiles were acquired. Also from geophysical and geochemical studies, 102 gas chimneys and ~50 gas flares were additionally recognized.

A gas flare being emitted from the seafloor can be identified using the echosounder system mounted on the vessel. Figure 2 shows numerous examples of gas flares in various shapes (i.e., linear, bent, or floated types). Some gas flares are quite extensive and appear to reach the sea surface.

In addition, a GSP-2 gravity hydrocorer with a length of 5.5 m was deployed on numerous occasions to collect sediment and gas hydrate samples. At Dungeon and Giselle sites, gas hydrates were recovered at ~390 mbsl, which is the shallowest occurrence in the Sea of Okhotsk to date (Fig. 3). The age of sediment recovered ranges from Late Pleistocene to Holocene (Greinert and Derkachev, 2004). Carbonate crusts/concretions and glendonite are frequently found within the sediment.

An interesting phenomenon that was observed during the marine survey is the dissociation of gas hydrate within the gravity hydrocorer as it was retrieved from the seafloor. Methane bubbles resulting from the dissociation of gas hydrate can be seen by the echosounder. Figure 2d is an example of gas flare coming out from the hydrocorer above relatively constant depth. By measuring the depth at which the gas flare appears on the echosounder images,

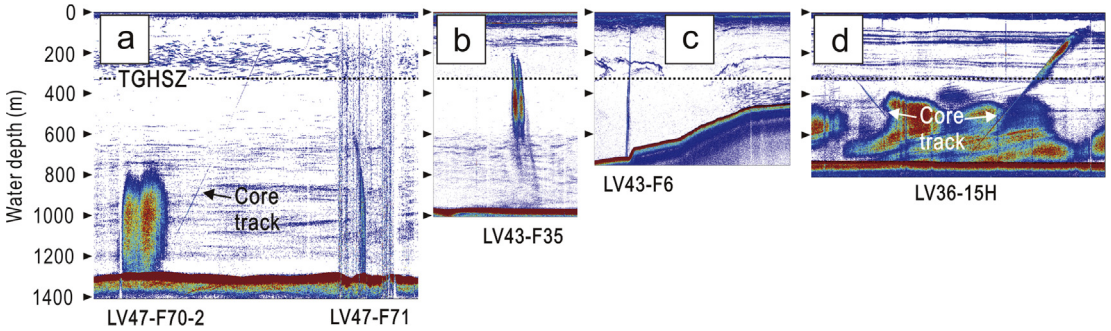


**Figure 2.** Gas flares as recorded by echosounder. The backscatter intensity is represented by colors from white for low to red for high. Reflection during the retrieval of cores can be seen (*core track*). The top of gas hydrate stability zone (*TGHSZ*) is depicted as a *dotted line*. Various shapes of gas flares are seen in (a), (b) and (c). (d) The depth where flare begins sometimes coincides with TGHSZ. (For interpretation of the references to color in this figure legend, the reader is referred to the web version of this article.)

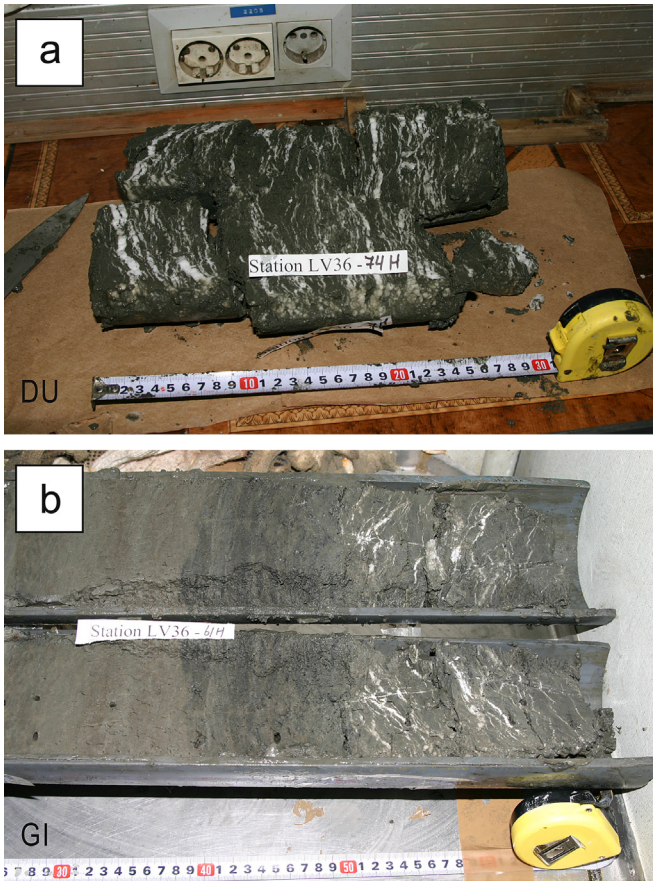


**Figure 3.** The picture of gas hydrate samples from sediment core. See Figure 1 for the location of the recovered gas hydrate samples. (a) From Dungeon (*DU*) and (b) from Giselle (*GI*) seepage structures are retrieved. The water depths at which these samples were recovered are repectively 385 and 390 mbsl.

one may obtain an indirect estimate of the top of the GHSZ in the water column.

The geothermal gradient that we used in this study was obtained during CHAOS-I project in 2003 (Table 1; Fig. 4). A violin-bow type GEOS-T thermo-probe having an accuracy of 2 mK/m on the geothermal gradient was deployed (Matveeva et al., 2005). The purpose of measuring heat flow at the time was to investigate if there is a meaningful variation in heat flux near the seepage sites. The survey was centered around the two main seepage sites.

**Table 1**
Heat flow measurements in the northeastern continental slope of Sakhalin Island during 2003 CHAOS survey using a marine heat probe after Matveeva et al. (2005). Eight measurements were made at different sites showing flare in the water column and seepage structure on the seafloor. To compare these sites with normal seafloor, two measurements were made at the reference sites.

| | Station (LV31-#HF) | Water depth (mbsl) | Geothermal gradient (mK/m) | Description of station |
|---|---|---|---|---|
| 1 | 06 | 763 | 34 | Reference site 1 |
| 2 | 18 | 967 | Failed | Flare 1 |
| 3 | 26 | 969 | Failed | Flare 1 |
| 4 | 35 | 957 | 144 | Flare 1 |
| 5 | 37 | 957 | 56 | Flare 1 |
| 6 | 38 | 958 | 64 | Flare 1 |
| 7 | 39 | 952 | 67 | Flare 1 |
| 8 | 40 | 953 | 249 | Flare 1 |
| 9 | 42 | 722 | 36 | Reference site 2 |
| 10 | 43 | 678 | 59 | Flare 2 |

In-situ thermal conductivity measurement could not be made at all sites due to instrumental failure.

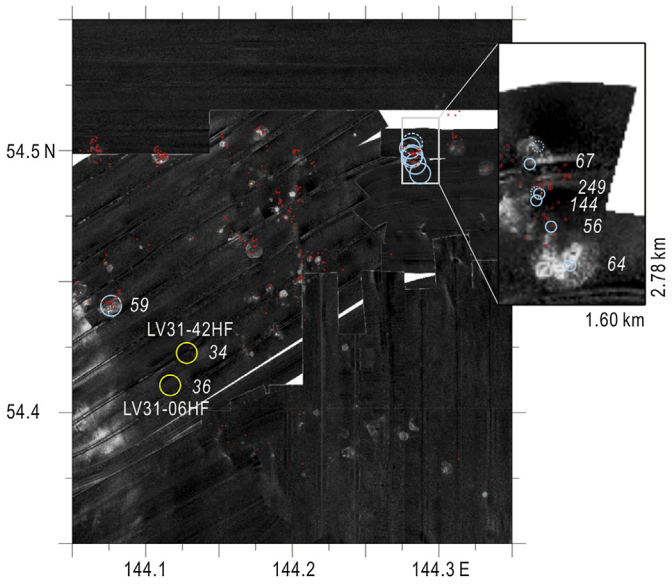


**Figure 4.** The location of heat flow measurements. Measurements at seepage structure are marked as *blue circles*, and those at non-seepage as *yellow circles* on top of side-scan sonar image where light area represents the region of high backscatter. *Dotted signs* represent failed measurements. The *red dots* indicate gas flares observed by the echosounder. Inset is a blow-up image of the *box*. The side-scan sonar image in the inset is the one below between overlapped two images. *Numbers in italic* represent geothermal gradient values. See Figure 1 for the location of the heat flow measurements. (For interpretation of the references to color in this figure legend, the reader is referred to the web version of this article.)

Unfortunately, 2 of the measurements failed and so did thermal conductivity measurements. In summary, 6 geothermal gradient measurements were made near the seepage structures, and 2 geothermal gradient measurements away from the seepage area for comparison. However, in this study, we utilize those 2 measurements that were taken for reference for background regional estimation, leaving out those taken near the seepage structures.

The presence of seepage structures can be readily recognized by examining the backscattering images of side-scan sonar (Fig. 4). High backscatter intensity shown as white in Figure 4 represents surface expression of seepage structures in this area (Baranov et al., 2008; Jin et al., 2011; Shoji et al., 2009, 2005). The side-scan sonar system used in this study had a frequency of 30 kHz and lateral resolution of greater than 2 m.

Another way to estimate the regional heat flow is to use BSR depths (e.g., Kim et al., 2010). This is because the BSR marks the base of the GHSZ, and therefore, its depth can be used as a proxy for regional heat flow. According to Yamano et al. (1982) who compared the BSR depths with actual heat flow observations in Nankai Trough, if done carefully, this approach has the advantage that it may provide an estimate on a regional scale. In our study area, the BSR is found extensively within the continental slope (Figs. 1b, c and 5), and therefore, the comparison between the observed and estimated BSRs may be important.

The BSRs were obtained during seismic experiment. We used SONIC-4 sparker system (500–2000 J in energy; 20–1200 Hz) as source and a single-channel streamer ($<\sim$50 m in active section length) as receiver. The vertical resolution and bottom penetration of the system are roughly 2–5 m and 50–300 m, respectively.

The water temperature and pressure information in the study area was obtained using CTD castings which have resolutions of 0.1 mK and 10 kPa, respectively. Three profiles are represented (Fig. 6). They exhibit the characteristic water temperature features in the Sea of Okhotsk.

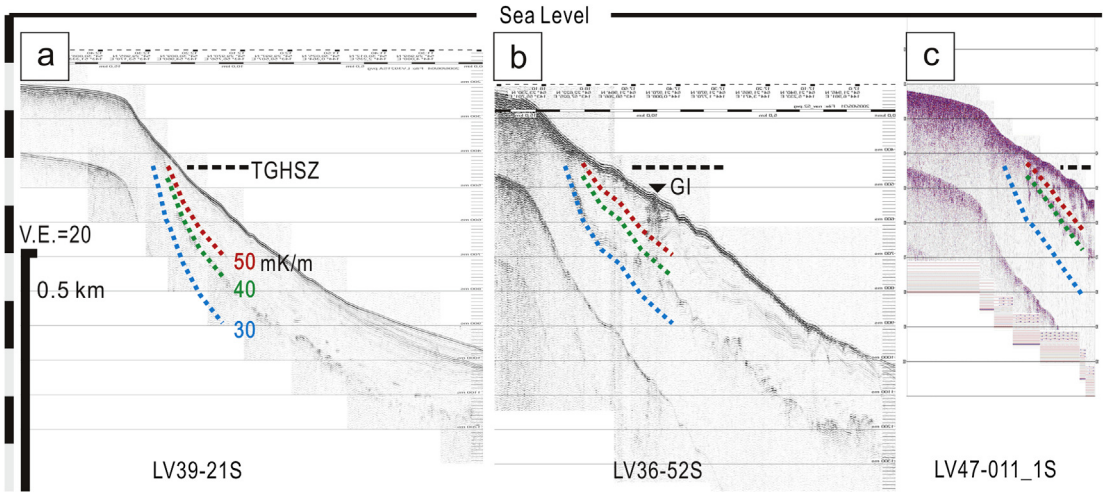


**Figure 5.** Seismic profiles showing the bottom-simulating reflectors (BSRs). The *dotted curves* represent estimated BSRs based on geothermal gradients of 30 (*blue*), 40 (*green*) and 50 (*red*) mK/m using the stability curve by Tishchenko et al. (2005). The *horizontal lines* indicate the top of gas hydrate stability zone (*TGHSZ*). Gas hydrate sample was taken at Giselle seepage structure (*GI*, *reverse triangle*), which is shown in Figure 3b. See Figure 1 for the location of the echosounder profiles. (For interpretation of the references to color in this figure legend, the reader is referred to the web version of this article.)

## 4. Thermal calculation

To understand the extent of GHSZ in the study area, we used the equation of Tishchenko et al. (2005) relating depth of base GHSZ to temperature and salinity, replacing the salinity variable by local value of 33.5‰ (Fig. 6). The relationship drawn from the intrinsic thermodynamic properties of methane and variations shows good agreement with reliable experiments widely used in gas hydrate community (e.g., Dickens and Quinby-Hunt, 1994; Brown et al., 1996). For instance, Lüdmann and Wong (2003) also used the equation of Dickens and Quinby-Hunt (1994) to assess the thickness of gas hydrate stability zone in the Sea of Okhotsk. They found a good agreement between estimated and observed BSR depths in the deep section of the Deryugin Basin.

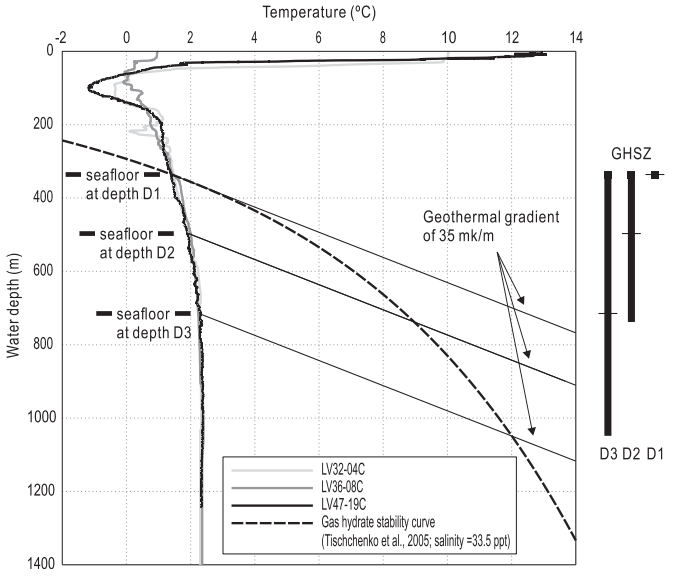


**Figure 6.** Water temperature profiles taken from three CTD stations. See Figure 1 for the location of CTD stations. Subzero temperature layer can be seen at 50–150 mbsl at all locations. The water temperature reaches a uniform value of ~2.2 °C below ~800 mbsl. Vertical *bars* represent gas hydrate stability zone (GHSZ) at water depths of D1, D2 and D3. For given water depths, the top and base of GHSZ can be determined by hydrotherm (*solid curves*), geotherm (*thin lines*), and gas hydrate stability curve (*dashed curve*). Note 1) that the base of GHSZ deepens with water depth deeper than D1 while the top of GHSZ is constant, and 2) that the GHSZ does not occur for water depth shallower than D1.

The relationship is based on a number of important assumptions. They include the conditions that methane should be concentrated beyond its maximum solubility and that the salinity and dissolved ion contents in the pore water should remain almost constant with respect to depth. Because numerous manifestations of gas are found in this area, we assume that the concentration of methane gas within the sediment is sufficiently high. The salinity in the water column ranges from 33 to 34‰ below 150 mbsl, and according to measurements taken from the cores, at least to a depth of several meters from the seafloor it is unchanged. The possibility that the salinity may change at greater depth within sediment exists and is a matter of concern. However, it is unknown at present. The content of dissolved ion was measured from the retrieved cores, but whether it varies as a function of depth and if so, how much have not been addressed.

Gas hydrate occurs under various environments and therefore it may be difficult to suppose that one single model or equation would explain all the features. For example, the regions where seepage structure and gas flare are present may differ from the 'normal' seafloor where they are absent. Conceptually, the input parameters may be distinguished into 'regional' and 'local' parameters. The pressure and background heat flow can be considered as regional parameters as they would vary little spatially on normal seafloor. On the other hand, factors such as capillarity due to grain size and pore water migration vary from locations to locations depending on the proximity of seepage structure. It is important to note that the thermal model in this study is used in the regional sense.

The regional parameters for the thermal model include pressure, temperature gradient, salinity and gas composition. The pressure can be directly obtained from the water depth and overlying sediment thickness. The sound velocities in water and sediments are set as 1450 and 1700 m/s, respectively. The former estimate is derived from the CTD measurements and the latter from DSDP Leg 19 in the Bering Sea (Creager et al., 1973). The reason to adopt the sound velocity in sediments in the Bering Sea is that it is the only result from direct measurement in the vicinity of Okhotsk Sea.

In this study, the thermal model is used once again to infer the stability of gas hydrate zone in the past and for the future. A similar attempt was made by Milkov and Sassen (2003) in the Gulf of Mexico where they assumed that the gas hydrates reach immediate equilibrium state after water temperature and sea level changes.

## 5. Present-day GHSZ

In the northeastern continental slope of Sakhalin Island, diverse manifestations of methane gas are found. Furthermore, some relationship can be seen among various features. For instance, hydroacoustic anomalies emitted from the seepage seem to disappear above certain elevation from the seafloor. An important element in understanding the nature of gas hydrate system is the extent of GHSZ in the water column and sediment.

The temperature profile is needed to determine the depth of GHSZ. The temperature within the water column was obtained at 3 CTD stations. The thermal gradient within the sediment is determined from a marine heat flow probe. The average background geothermal gradient at our study area, not affected by advective flow at the seepage, is 35 mK/m.

For a given temperature profile, the GHSZ may lie within the water column or in the sedimentary pile (Cases D2 and D3 in Fig. 6) or just on the seafloor (Case D1 in Fig. 6) depending on water depth. In any case, the top of GHSZ is constant while the base of GHSZ deepens with water depth. In the study area, we obtained 322 mbsl as the top of GHSZ using the equation of Tishchenko et al. (2005) with parameter values above. In addition, the estimated top of GHSZ may be compared with two types of observation: 1) the flares as seen by echosounders as the sediment sample containing gas hydrate is retrieved from the seafloor (Fig. 2d), and 2) the point at which the BSR intersects the seafloor as seen in the seismic sections (Fig. 5).

In our study area, the depth of BSR below the seafloor becomes greater with water depth. The BSRs generally resemble topography of the seafloor except in the case where they are interrupted by seepage structures. Around seepage structures, the shape of BSR in general becomes concave upward (Fig. 5b). At shallow depth, the BSR depth becomes so shallow that it intersects the seafloor. In our study area, such intersection occurs at ~290 mbsl (Fig. 5). This means that there is about 10% difference between the observation and our estimation.

The estimated top of GHSZ can be compared with the depth where dissociation occurs as hydrate sample is retrieved. This can be done by measuring the appearance and disappearance of flare on echosounder records. According to our observations during retrieval of sediment cores, the flares occur at ~320 mbsl, matching well with the estimation. On the other hand, disappearing depth of gas flare triggered naturally on the seafloor does not necessarily match with the estimated depth of GHSZ top.

The bottom of GHSZ needs to be examined as well. Figure 5 shows that estimated BSR locations based on different geothermal gradient values. Observed BSRs reside between locations of 30 and 40 mK/m and seem to decrease in deepening toward basin. This may suggest that in the study area, BSR-derived geothermal gradient is consistent with the averaged background geothermal gradient of 35 mK/m, and that the actual geothermal gradient slightly increases to the basin in terms of P–T relationship of gas hydrate stability. The exact cause of that slight shoaling of BSR to the basin is not clear at this stage. On the other hand, BSR depth seems to shoal up slightly near the seepage structures (see BSR below GI seepage structure in Fig. 5b). This may indicate that advective fluid take an important role to transfer heat, at least for deep sedimentary section, at the GI structure (see Section 6.1).

Gas hydrates were sampled at several sites in study area (*stars* in Fig. 1). They occur in various types of lenticular bed, microaggregate, vein/void-filling, and massive chunk (Mazurenko et al., 2005). The Dungeon seepage structure has the shallowest occurrences of natural gas hydrate at 385 mbsl, which shows up as lenticular-bedded or vein types over a 30 cm-thick sediment interval (Fig. 3a). The second shallowest one is at the Giselle structure in 390 mbsl (Fig. 3b), indicating gas hydrate occurrence at shallow depths is not rare in the study area. These occurrence depths are not much deeper than the estimated top of GHSZ.

A comparison between the observed GHSZ marked by manifestations of methane and the estimated GHSZ exhibits a good agreement, suggesting that the present-day GHSZ in the study is well defined by P–T conditions. This can be the key to consider the extent of GHSZ in the past and near-future based on information on water temperature and sea level at that time.

## 6. Discussion

### 6.1. Estimating the regional geothermal gradient

Conventional heat flow measurements are subject to a large variability because they can be affected by irregularities on or near the seafloor such as cracks or fluid circulation within sediment. To compensate for such variability, a number of measurements are often made and then averaged to represent the regional or background heat flow. In our study area, seepage structures present such irregularity, and therefore a distinction should be made between the thermal gradients measured on the seepage sites and those taken in the non-seepage sites.

Among the 8 successful geothermal gradient measurements conducted in this region, 6 were taken at the seepage sites and 2 were made on the normal seafloor (Table 1; Fig. 4). The latter were made for the purpose of comparison between the seepage and non-seepage sites. There is a contrast between the two types of sites. In general, the geothermal gradient at seepage sites is not only higher than that of non-seepage sites but also exhibits a larger variation. For instance, thermal gradient values as high as 249 mK/m and low as 56 mK/m were found at the seepage sites whereas the two non-seepage sites showed 34 and 36 mK/m.

The difference between the seepage and non-seepage sites may be explained by the difference in the importance of conductive versus convective heat transfer below the seafloor (Fig. 7). Three different cases are depicted. In the normal seafloor where there is no seepage structure (Case 1 in Fig. 7a), conductive cooling is probably the dominant mode of heat transfer. The temperature profile can be represented as a single line whose slope corresponds to the regional geothermal gradient. This is depicted as blue Line 1 (in the web version) in Figure 7b. On the other hand, seepage would be a transient and dynamic feature on the seafloor. Therefore, instead of representing it as a single temperature profile, we need to consider the two end-member cases, one where gas is rising up and causing a flare (Case 3 in Fig 7a), and the other where the seepage site is in quiescent mode (Case 2 in Fig. 7a).

In the case of gas venting (Case 3 in Fig. 7a), convection would be the dominant mode of heat transfer (shown as orange Line 3 (in the web version) in Fig. 7b). The upwelling would not stop at a certain depth below the seafloor and would rise into the water column, as evidenced by gas flares. The temperature of fluid venting out would be higher than the bottom water temperature. The geothermal gradient corresponding to the convection (Line 3) would be gentler than that of conduction (Line 1).

After burst of gas flares, we envisage that the seepage sites would enter into dormant period where the region of upwelling is confined to a certain depth below the seafloor (Case 2 in Fig. 7a).

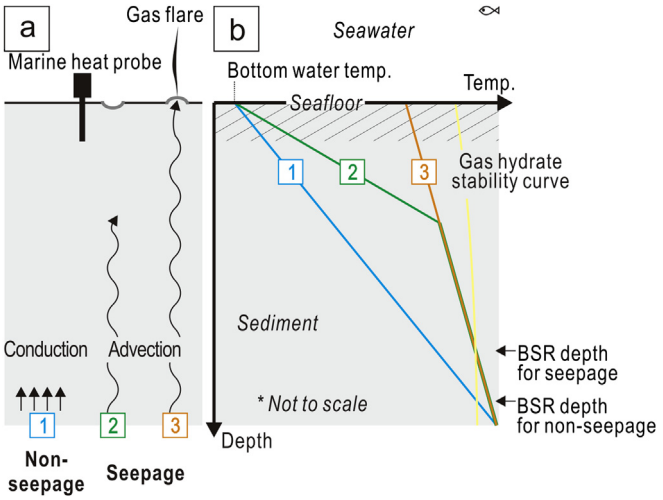


**Figure 7.** A schematic diagram illustrating the difference in heat transfer process and resulting thermal structure at non-seepage and seepage sites. (a) The dominant heat transfer process may vary between at a non-seepage site and at a seepage site. At a non-seepage site, conduction would be the dominant mode of heat transfer (Case *1*). On the other hand, at a seepage site, convection by advective flow may play an important role. In the case of active venting, the warm fluid would rise up quickly to the surface (Case *3*). Once the active venting has ceased, the convective fluid would not reach the seafloor and may be confined to the deeper portions of the sedimentary layer (Case *2*). The sedimentary section may be divided into two: the upper part where conduction is dominant and the lower part where convection is dominant. (b) The local temperature profiles would depend on the dominant heat processes. The temperature profile for active venting (Line *3*) at the seepage site may be less steep than that at the non-seepage sites (Line *1*). Hence, BSR depth can shoal up at the seepage site compared to at the non-seepage site for given *gas hydrate stability curve*. In the case of active venting, the fluid venting out at the seafloor would be much warmer than the bottom water temperature. Depending on whether the seepage venting is active or inactive, the geothermal gradient may differ. When the active venting has ceased, the temperature profile at the seepage site may be shown a line bent at the depth where the convective fluid reaches (Line *2*). Thus, the geothermal gradient corresponding to the conduction-dominant upper part is steeper than that to the convection-dominant lower part. Also, the geothermal gradient observed at the inactive or dormant seepage site becomes higher than that at the non-seepage site because a *marine heat probe* can penetrate into the topmost several meters below the seafloor (*hatched area*).

Above this depth, the conduction becomes the dominant mode of heat transfer. As a result, the temperature profile may be depicted as green Line 2 (in the web version) in Figure 7b. This conceptual model may explain the difference in the geothermal characteristics between seepage and non-seepage structures. Because the heat measurement was confined to a few meters below the seafloor (hatched area in Fig. 7b), the geothermal gradient at the seepage structure can be higher than that of the normal seafloor depending on the seepage activity. The transient nature of seepage structure may also explain its greater geothermal variability (Table 1).

According to our hypothesis, geothermal gradient value lower than 35 mK/m of the normal seafloor (Case 1 in Fig 7a), combined with an anomalous high value of seafloor temperature, should be yielded at the actively-venting seepage structure (Case 3 in Fig. 7a), but such data was not obtained in the survey. This is partly because an attempt to measure the geothermal gradient at the actively-venting seepage structure was not made considering unexpected damage to an instrument although the purpose of measurements is to see variation near seepage structures. It will become an interesting topic further to validate our hypothesis through geothermal gradient measurements just at the actively-venting structure as done in the coring to retrieve gas hydrate samples as shown in Figure 2d.

The acoustic blank features that were observed beneath many seepage structures during seismic and subbottom profiler surveys in this region may correspond to the zone of convections beneath the seepage structures (Jin et al., 2011). As noted earlier, the BSR depth becomes shallower beneath the seepage structures when compared with the normal seafloor. This perturbation in the BSR depth is illustrated in Figure 7b in terms of change in depth where the local geotherm intersects the gas hydrate stability curve (shown as yellow curve (in the web version) in Fig. 7b).

Since the main purpose of this study is to understand the extent of GHSZ, we ignore anomalous regions of geothermal gradient associated with seepage structures and only consider the two measurements taken on the normal seafloor as background geothermal gradient. One of the important sources of error associated with heat flow is the thermal conductivity, a property of the material which is multiplied by the geothermal gradient to produce heat flux value. Kim et al. (2010) have shown that depending on how the thermal conductivity was measured, using in-situ device or from retrieved core samples, the values can vary by as much as 40%. They argued that much of the uncertainties in heat flow experiments may come from inaccurate estimation of thermal conductivity. Fortunately, the model used in this study requires geothermal gradient as input parameter and does not involve thermal conductivity information, which failed on all stations according to Matveeva et al. (2005).

### 6.2. Past slope failure during the Last Glacial Maximum

A large difference in morphology exists between the north and south of the continental slope (Fig. 8). While the slope to the north of the LFZ is concave-upward, it is convex-upward to the south. The difference is thought to be a direct consequence of massive slope failure in the northern slope (Wong et al., 2003). According to their estimate, the volume of sediment corresponding to the submarine landslide is as large as 660 km$^3$.

A major source of debate is the timing of the slope failure. Wong et al. (2003) argue that the slope failure occurred pre-Uppermost

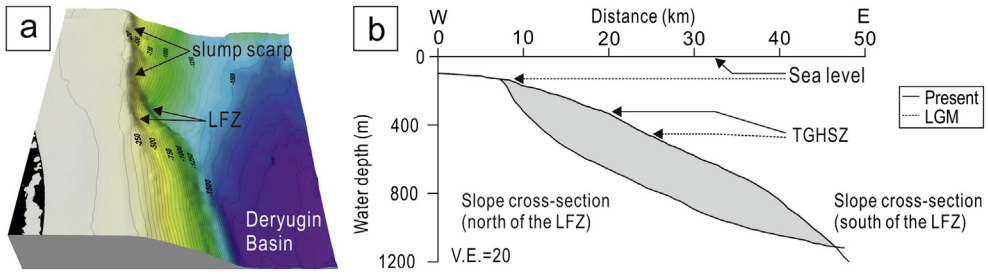


**Figure 8.** The comparison of the slope between the continental margin to the north and south of the Lavrentyev Fault Zone (*LFZ*) (modified from Wong et al., 2003). (a) 3-Dimensional aerial view. See *Slump scarp* develops along contour lines 250–300 mbsl. See Figure 1 for the location. (b) *Sea level* and the top of gas hydrate stability zone (*TGHSZ*) are represented for present-day (*solid lines*) and the Last Glacial Maximum (*LGM*; *dotted lines*).

Pleistocene (earlier than at least 350 ka) based on the finding that sedimentary cores obtained during the KOMEX project show good correlation down to 350 ka on isotopic and stratigraphic investigations.

However, in this study, we suggest that the slope failure may have occurred much later than initially proposed, perhaps as late as 20 ka. Our argument is based on the analysis of subbottom profiler data which was collected in 2006. The detailed examination of the subbottom profile reveals a new reflection within the sediment (Fig. 9). Observations and circumstantial evidences suggest the reflector may be the top surface of glided mass. For instance, the acoustic character is quite different between the sediment layer above the reflector and the layer below. Sediment layer overlying above the reflector is transparent/reflector-poor. Its thickness is variable (~10–40 m) depending on irregularity of the reflector: rather constant at area underlain by flat reflector (Fig. 9a) or thinning-away offshore with pinching-out at the top of highs/bumps (Fig 9b). These characteristics indicate that the transparent facies mostly consists of hemipelagite with some turbidite. On the other hand, good parallel reflectors below the reflector are not continuous, but deformed in some places along the profile, which supports sliding/slumping process. The more deformed the weaker/fewer reflectors below the top surface of glided mass could be distinguished on the profile. Thus, the strong reflector highs with absence of reflectors below (e.g., at 2.5 and 3.5 km in the profile in Fig. 9b) are not rafted blocks poking through the hemipelagic cover, but represent the same strongly deformed glided mass. Lastly, a similar reflector is not found in subbottom profiles to the south of the LFZ at this stage. Based on evidence above, such reflector is interpreted to mark the boundary between mass wasted deposit Wong et al. (2003) claimed and hemipelagite layer that has gradually settled on top.

A crucial piece of information in determining the timing of landslide is the average sedimentation rate around the region. The sedimentation rate within Sea of Okhotsk is quite variable with time and location. At the northeastern continental slope, the averaged sedimentation rate for the sediment deposited since the uppermost Pleistocene ranges 40 cm/kyr to over 100 cm/kyr (Biebow et al., 2003; Gorbarenko et al., 2010). Also as shown earlier (Fig. 9b), the thickness of the hemipelagite layer varies depending on the distance from the coast line. In this study, we use the sedimentation rate of 100 cm/kyr as reported by Biebow et al. (2003) which was obtained by measuring Holocene deposits from tens of sites on the slope. If we use this value, the estimated timing of landslide is roughly 20 ka. Hence, the timing of landslide is consistent with that of the Last Glacial Maximum (LGM).

It is important to check whether gas dissociation during the LGM may have led to the actual slope failure. We examine the GHSZ based on paleo-environmental information including past temperature and pressure. Again, the model by Tishchenko et al. (2005) is used to determine the extent of GHSZ.

The bottom water temperature and salinity during the LGM can be roughly estimated based on oxygen isotope analysis of benthic foraminifera selected from sediment cores in the Okhotsk Sea and the northwestern Pacific. During the LGM, $\delta^{18}O$ ranges from 4.5 to 5.5‰ which is slightly higher than in the Holocene (Keigwin, 1998). The variation may be attributed to change in temperature and salinity. However, the salinity itself changed little during the LGM (Lüdmann and Wong, 2003; Oba and Murayama, 2004) and therefore most of the variation in $\delta^{18}O$ may have been caused by changes in temperature and ice volume. After correcting for the ice volume effect of 1.3‰ following Fairbanks (1989), we argue that the temperature of the deep water mass lying above 1500 m during the LGM may have been quite similar to that of present-day water mass lying at 1000 m. Therefore, the temperature for deep water during the LGM is inferred from that of the present-day water mass lying at 1000 m in the Sea of Okhotsk.

The temperature of water at the sea surface during the LGM may be estimated from ice-rafted debris information. Sakamoto et al. (2005) found ice-rafted debris through the whole western Okhotsk Sea. We infer from such findings that, like present day, a low temperature water layer exists at intermediate depth resulting from seasonal ice extension and contraction. In other words, the temperature profile at shallow depths during the LGM may have been quite similar to that of present day.

To determine the ambient pressure within GHSZ during the LGM, we need to estimate the sea level. In this study, only the eustatic sea level drop of ~130 m (Clark et al., 2009; Miller et al.,

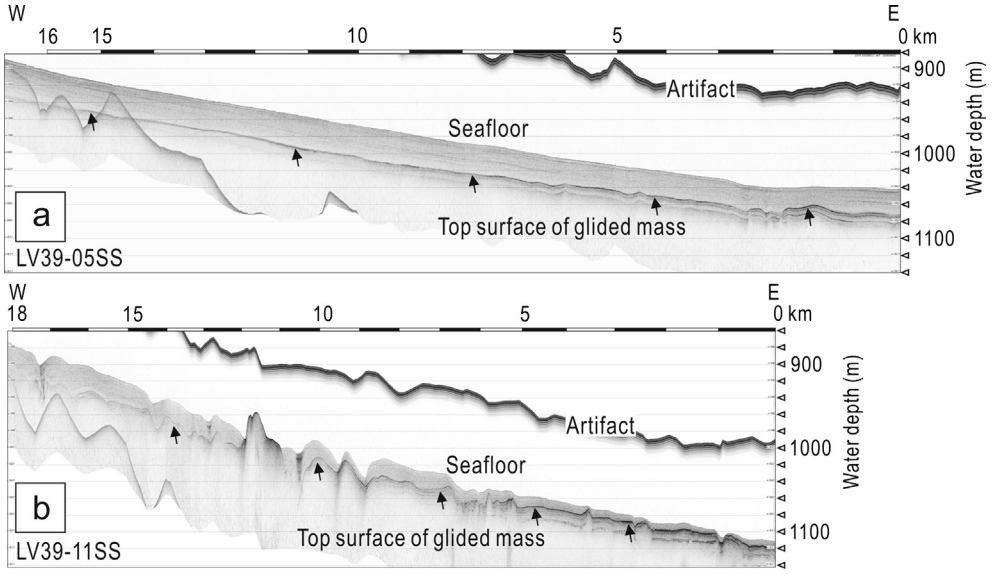


**Figure 9.** Subbottom profiles showing a clear top surface of glided mass (*arrows*) at ~10–40 m below the seafloor. The more deformed the less reflectors below the top surface of glided mass could be distinguished. Thickness of hemipelagite over the top surface is variable due to irregularity of the glided mass top surface: (a) rather constant at area with the flat top surface, and (b) thin or absent over highs/bumps as well as thinning-away offshore. See Figure 1 for the location of the subbottom profiles.

2005) is considered. This is because in the study area there is a little information on relative sea level change. For instance, as a proxy of the lowstand during the LGM even the depth of shelf break is ambiguous at around the Sakhalin Island.

Using the past temperature and pressure information, the top of GHSZ during the LGM can be predicted (Fig. 8). According to our calculation, the top of GHSZ during the LGM should lie at 450 mbsl with respect to the present-day sea level. This depth corresponds to the middle of the slope-failed section (Fig. 8). At first glance, this may be perplexing because only the region above the top of GHSZ can have undergone dissociation and yet the region of failure was much more extensive upslope.

Slope failure of hydrate-bearing sediments led by gas hydrate dissociation below the top of GHSZ has been reported at continental margins. For instance, the well-documented Storegga Slide in the Norwegian continental margin shows widespread slide/slump below the top of GHSZ at glacial period, triggered by an earthquake combined with gas hydrate dissociation (Bugge et al., 1987; Haflidason et al., 2004). According to Haflidason et al. (2004) and Sultan et al. (2004), the slope failure occurred initially downslope below the top of GHSZ due to dynamic dissociation of gas hydrate according to gas concentration change and progressed upslope.

However, slope failure extending to non-hydrate bearing upslope as occurred in the study area has not been documented well yet. We do not know the exact mechanism for such propagation of destabilization to upslope at this stage due to lack of data. We speculate that frequent small earthquakes in the study area at the vicinity of plate boundary (Fig. 1a) may lead to subsequent and/or coincident slope failure extending to non-hydrate bearing area. Furthermore, considering the catastrophic nature of slope failure (e.g., Puzrin and Germanovich, 2005; McIver, 1982), it is not unreasonable to suggest that the dissociation of gas hydrate in the section below 450 mbsl was an important factor that led to the landslide of the entire section of the northern slope.

## 7. Conclusions

A numerous set of measurements including seismic, oceanographic, hydroacoustic, heat flow, and sedimentary data were obtained in the northeastern continental slope of Sakhalin Island during CHAOS (hydro-Carbon Hydrate Accumulation in the Okhotsk Sea) and SSGH (Sakhalin Slope Gas Hydrate) projects. Using a simple model, we estimated the stability of gas hydrate zone and compared it with observed gas hydrate features in the sediment and the water column.

The heat flow (geothermal gradient) values obtained in this region can be divided into those taken near the seepage structures and those from the normal seafloor as reference. We suggest that the latter is more representative for the background heat flow (geothermal gradient). Our study finds that the depth of BSR and the initiation of gas flares from a retrieved core in the water column are consistent with gas hydrate stability zone (GHSZ) estimated using the regional geothermal gradient value of 35 mK/m and the sea water temperature profile.

An important feature in this area is the large concave-upward slope sections to the north of the LFZ, which was interpreted as a product of major landslide. Previously Wong et al. (2003) suggested the timing of the landslide as older than 350 ka. The timing of the landslide is reestimated in the light of subbottom profiler data which show a new horizontal reflector. The horizon is interpreted as the top surface of glided mass marking the boundary between landslide deposit and hemipelagic sediment layer that has settled on top since the slope failure. Using the sedimentation rate of $>$100 cm/kyr, we suggest that the mass wasting occurred at 20 ka, which coincides with the late stage of the Last Glacial Maximum. On the other hand, the reason for slope failure extending to non-hydrate-bearing sediments upslope remains speculative at this stage.

## Acknowledgments

We would like to appreciate Drs. Johannes Wendebourg (the editor) and Patrice Imbert (the Reviewer #2) for their thoughtful comments and valuable suggestions to help us to improve the manuscript. We also thank the captain and crew of the R/V *Akademik M. A. Lavrentyev*, and all participants of the CHAOS and SSGH projects. This work was supported by KOPRI (Grants PM12020 and PN12020) as well as MEST (No. 2009-0092790). Also this research was a part of the project titled "Heat flow study of deep-drilled sedimentary cores from Canterbury Basin, New Zealand (Exp. 317) and geomagnetic study of lower crustal gabbros in superfast spreading zone in eastern Pacific (Exp. 335)" funded by the Ministry of Land, Transport and Maritime Affairs, Korea. Y.-G. Kim was supported by the BK21 Program at Seoul National University as part of Ph. D. research. This study was conducted in international collaboration supported by Japan Society for the Promotion of Science KAKENHI 23254008 and Presidium of Russian Academy of Sciences, Programme No. 20.

## References

Astakhov, A.S., Vagina, N.K., Gorbarenko, S.A., Demidenko, E.L., shapovalov, V.V., Birulina, M.G., 1998. Holocene sediment rates in the Okhotsk Sea. Tikhookeanskaya Geology 4, 3–14.

Baranov, B., Wong, H.K., Dozorova, K., Karp, B., Ludmann, T., Karnaukh, V., 2002. Opening geometry of the Kurile Basin (Okhotsk Sea) as inferred from structural data. Island Arc 11, 206–219.

Baranov, B.V., Jin, Y.K., Shoji, H., Obzhirov, A., Dozorova, K.A., Salomatin, A., Gladysh, V., 2008. Gas Hydrate System of the Sakhalin Slope: Geophysical Approach. Scientific Report of the Sakhalin Slope Gas Hydrate Project 2007. KOPRI.

Biastoch, A., Treude, T., Rüpke, L.H., Riebesell, U., Roth, C., Burwicz, E.B., Park, W., Latif, M., Böning, C.W., Madec, G., Wallmann, K., 2011. Rising Arctic Ocean temperatures cause gas hydrate destabilization and ocean acidification. Geophysical Research Letters 38, L08602. http://dx.doi.org/10.1029/2011GL047222.

Biebow, N., Kulinich, R., Baranov, B., 2003. Cruise Report: KOMEX (Kurile Okhotsk Sea Marine Experiment) RV Akademik M. A. Lavrentyev cruise 29 Leg 1 and Leg 2, GEOMAR Report. Research Center for Marine Geosciences, p. 190.

Bouriak, S., Vanneste, M., Saoutkine, A., 2000. Inferred gas hydrates and clay diapirs near the Storegga Slide on the southern edge of the Vøring Plateau, offshore Norway. Marine Geology 163, 125–148.

Brown, K.M., Bangs, N.L., Froelich, P.N., Kvenvolden, K.A., 1996. The nature, distribution, and origin of gas hydrate in the Chile Triple Junction region. Earth and Planetary Science Letters 139, 471–483.

Bugge, T., Befring, S., Belderson, R.H., Eidvin, T., Jansen, E., Kenyon, N.H., Holtedahl, H., Sejrup, H.P., 1987. A giant three-stage submarine slide off Norway. Geo-Marine Letters 7, 191–198.

Cha, S.B., Quar, H., Wilderman, T.R., Sloan, E.D., 1988. A third-surface effect on hydrate formation. The Journal of Physical Chemistry 92, 6492–6494.

Clark, P.U., Dyke, A.S., Shakun, J.D., Carlson, A.E., Clark, J., Wohlfarth, B., Mitrovica, J.X., Hostetler, S.W., McCabe, A.M., 2009. The Last Glacial Maximum. Science 327, 710–714.

Collett, T.S., 2002. Energy resources potential of natural gas hydrates. American Association of Petroleum Geologists Bulletin 86, 1971–1992.

Creager, J.S., Scholl, D.W., Party, D.L.S.S., 1973. Initial Reports of the Deep Sea Drilling Project Leg 19. Washington, DC.

de Roo, J.L., Peters, C.J., Lichtenthaler, R.N., Diepen, G.A.M., 1983. Occurrence of methane hydrate in saturated and unsaturated solutions of sodium chloride and water in dependence of temperature and pressure. AIChE Journal 29, 641–657.

Dickens, G.R., Quinby-Hunt, M.S., 1994. Methane hydrate stability in seawater. Geophysical Research Letters 21, 2115–2118.

Dickens, G.R., Quinby-Hunt, M.S., 1997. Methane hydrate stability in pore water: a simple theoretical approach for geophysical applications. Journal of Geophysical Research 102, 773–783.

Fairbanks, R.G., 1989. A 17,000-year glacio-eustatic sea level record: influence of glacial melting rates on the Younger Dryas event and deep-ocean circulation. Nature 342.

Gorbarenko, S.A., Khusid, T.A., Basov, I.A., Oba, T., Southon, J.R., Koizumi, I., 2002a. Glacial Holocene environment of the southeastern Okhotsk Sea: evidence from

geochemical and palaeontological data. Palaeogeography, Palaeoclimatology, Palaeoecology 177, 237–263.
Gorbarenko, S.A., Nürnberg, D., derkachev, A.N., Astakhov, A.S., Southon, J.R., Kaiser, A., 2002b. Magnetostratigraphy and tephrochronology of the Upper Quaternary sediments in the Okhotsk Sea: implication of terrigenous, volcanogenic and biogenic matter supply. Marine Geology 183, 107–129.
Gorbarenko, S.A., Psheneva, O.Y., Artemova, A.V., Matul, A.G., Tiedemann, R., Nürnberg, D., 2010. Paleoenvironment changes in the NW Okhotsk Sea for the last 18 kyr determined with micropaleontological, geochemical, and lithological data. Deep-Sea Research I 57, 797–811.
Greinert, J., Derkachev, A.N., 2004. A glendonites and methane-derived Mg-calcites in the Sea of Okhotsk, Eastern Siberia: implications of a venting-related ikaite/glendonite formation. Marine Geology 204, 129–144.
Hachikubo, A., Krylov, A., Sakagami, H., Minami, H., Nunokawa, Y., Shoji, H., Matveeva, T., Jin, Y.K., Obzhirov, A., 2009. Isotopic composition of gas hydrate in subsurface sediments from offshore Sakhalin Island, Sea of Okhotsk. Geo-Marine Letters. http://dx.doi.org/10.1007/s00367-00009-00178-y.
Haflidason, H., Sejrup, H.P., Nygård, A., Mienert, J., Bryn, P., Lien, R., Forsberg, C.F., Berg, K., Masson, D., 2004. The Storegga Slide: architecture, geometry and slide development. Marine Geology 213, 201–234.
Jin, Y.K., Kim, Y.-G., Baranov, B., Shoji, H., Obzhirov, A., 2011. Distribution and expression of gas seeps in a gas hydrate province of the northeastern Sakhalin continental slope, Sea of Okhotsk. Marine and Petroleum Geology 28, 1844–1855.
Jin, Y.K., Obzhirov, A., Shoji, H., Mazurenko, L., 2007. Hydro-carbon Hydrate Accumulations in the Okhotsk Sea (CHAOS-III Project): Report of R/V Akademik M. A. Lavrentyev Cruise 39. Korea Polar Research Institute, Incheon, p. 132.
Jin, Y.K., Shoji, H., Baranov, B., Obzhirov, A., 2008. Operation Report of Sakhalin Slope Gas Hydrate Project 2008: R/V Akademik M. A. Lavrentyev Cruise 44. Korea Polar Research Institute, KORDI, Incheon, p. 64.
Katsuki, K., Khim, B.-K., Itaki, T., Okazaki, Y., Ikehara, K., Shin, Y., Yoon, H.I., Kang, C.Y., 2010. Sea-ice distribution and atmospheric pressure patterns in southwestern Okhotsk Sea since the Last Glacial Maximum. Global and Planetary Change 72, 99–107.
Keigwin, L.D., 1998. Glacial-age hydrography of the far northwest Pacific Ocean. Paleoceanography 13, 323–339.
Kennett, J.P., Cannariato, K.G., Hendy, I.L., Behl, R.J., 2000. Carbon isotopic evidence for methane hydrate instability during quaternary interstadials. Science 288, 128–133.
Kharakhinov, V.V., 1998. Tectonics of the Okhotsk Sea Oil and Gas Potential Province. SakhalinNIPImorneft, Okha.
Kharakhinov, V.V., 2010. Oil and Gas Geology of the Sakhalin Region. Scientific World Publ., Moscow.
Kim, Y.-G., Lee, S.-M., Matsubayashi, O., 2010. New heat flow measurements in the Ulleung Basin, East Sea (Sea of Japan): relationship to local BSR depth, and implications for regional heat flow distribution. Geo-Marine Letters 30, 595–603.
Kitani, K., 1973. An oceanographic study of the Sea of Okhotsk particularly in regard to cold waters. Bulletin of Far Seas Fishery Research Laboratory 9, 45–77.
Kvenvolden, K.A., 1998. A primer on the geological occurrence of gas hydrate. In: Henriet, J., Mienert, J. (Eds.), Gas Hydrates: Relevance to World Margin Stability and Climatic Change. The Geological Society, pp. 9–30.
Lüdmann, T., Wong, H.K., 2003. Characteristics of gas hydrate occurrences associated with mud diapirism and gas escape structures in the northwestern Sea of Okhotsk. Marine Geology 201, 269–286.
Matsumoto, R., Ryu, B.-J., Lee, S.-R., Lin, S., Wu, S., Sain, K., Pecher, I., Riedel, M., 2011. Occurrence and exploration of gas hydrate in the marginal seas and continental margin of the Asia and Oceania region. Marine and Petroleum Geology 28, 1751–1767.
Matveeva, T., Soloviev, V., Shoji, H., Obzhirov, A., 2005. Hydro-carbon Hydrate Accumulations in the Okhotsk Sea (CHAOS Project Leg I and Leg II): Report of R/V Akademik M. A. Lavrentyev Cruise 31 and 32. St. Petersburg, p. 164.
Mazurenko, L., Soloviev, V., Matveeva, T., Shoji, H., Kaulio, V., Logvina, E., Minami, H., Hachikubo, A., Sakagami, H., 2005. Methane Venting on the Continental Margin off NE Sakhalin: Nature of Gas, Authigenic Carbonates and Gas Hydrates. European Geosciences Union.
Mazurenko, L.L., 2006. Hydro-carbon Hydrate Accumulations in the Okhotsk Sea (CHAOS-II Project): Report of R/V Akademik M. A. Lavrentyev Cruise 36. VNIIOkeangeologia. Vladivostok-St.Petersburg, p. 127.
McIver, R.D., 1982. Role of naturally occurring gas hydrates in sediment transport. The American Association of Petroleum Geologists Bulletin 66, 789–792.
Milkov, A.V., Sassen, R., 2003. Two-dimensional modeling of gas hydrate decomposition in the northwestern Gulf of Mexico: significance to global change assessment. Global and Planetary Change 36, 31–46.
Miller, K.G., Kominz, M.A., Browning, J.V., Wright, J.D., Moutain, G.S., Katz, M.E., Sugarman, P.J., Cramer, B.S., Christie-Blick, N., Pekar, S.F., 2005. The Phanerozoic record of global sea-level change. Science 310, 1293–1298.
Oba, T., Murayama, M., 2004. Sea-surface temperature and salinity changes in the northwest Pacific since the Last Glacial Maximum. Journal of Quaternary Science 19, 335–346.
Obzhirov, A., Shakirov, R., Salyuk, A., Suess, E., Biebow, N., Salomatin, A., 2004. Relations between methane venting, geological structure and seismo-tectonics in the Okhotsk Sea. Geo-Marine Letters 24, 135–139.
Paull, C.K., Ussler III, W., Dillon, W.P., 2000. Potential role of gas hydrate decomposition in generating submarine slope failures. In: Max, M.D. (Ed.), Natural Gas Hydrate in Oceanic and Permafrost Environments. Kluwer Academic Publishers, Dordrecht, pp. 146–156.
Puzrin, A.M., Germanovich, L.N., 2005. The growth of shear bands in the catastrophic failure of soils. Proceedings of the Royal Society A: Mathematical, Physical and Engineering Sciences 461, 1199–1228.
Rodnikov, A.G., Sergeyeva, N.A., Zabarinskaya, L.P., 2002. The Deep Structure of the Deryugin Basin (the Sea of Okhotsk), EGS XXVII. General Assembly, Nice.
Sakamoto, T., Ikehara, M., Aoki, K., Iijima, K., Kimura, N., Nakatsuka, T., Wakatsuchi, M., 2005. Ice-rafted debris (IRD)-based sea-ice expansion events during the past 100 kyrs in the Okhotsk Sea. Deep-Sea Research II 52, 2275–2301.
Shoji, H., Jin, Y.K., Obzhirov, A., 2008. Operation Report of Sakhalin Slope Gas Hydrate Project 2007: R/V Akademik M. A. Lavrentyev Cruise 43. Kitami Institute of Technology, New Energy Resources Research Center, Kitami, p. 39.
Shoji, H., Jin, Y.K., Obzhirov, A., Baranov, B., 2010. Operation Report of Sakhalin Slope Gas Hydrate Project 2009: R/V Akademik M. A. Lavrentyev Cruise 47. Kitami Institute of Technology, New Energy Resources Research Center, Kitami, p. 136.
Shoji, H., Jin, Y.K., Obzhirov, A., Salomatin, A., Baranov, B., Gladysch, V., Hachikubo, A., Minami, H., Yamashita, S., Takanashi, N., 2009. Methane hydrates and plumes in the Sea of Okhotsk. Journal of Geography 118, 175–193.
Shoji, H., Soloviev, V., Matveeva, T., Mazurenko, L., Minami, H., Hachikubo, A., Sakagami, H.K.H., Kaulio, V., Gladysch, V., Logvina, E., Obzhirov, A., Baranov, B., Khlystov, O., Biebow, N., Poort, J., Jin, Y.K., Kim, Y., 2005. Hydrate-bearing structures in the Sea of Okhotsk. EOS 86, 13–24.
Sloan, E.D.J., 1990. Clatrhate Hydrates of Natural Gases. Marcel Dekker, New York.
Sultan, N., Cochonat, P., Foucher, J.-P., Mienert, J., 2004. Effect of gas hydrates melting on seafloor slope instability. Marine Geology 213, 379–401.
Talley, L.D., Nagata, Y., 1995. The Sea of Okhotsk and Oyashio Region. 2. North Pacific Marine Science Organization (PICES), Sidney, BC.
Tanaka, A., Yamano, M., Yano, Y., Sadada, M., 2004. Geothermal Gradient and Heat Flow Data in and Around Japan, Digital Geoscience Map DGMP-5. Geological Survey of Japan, AIST, Tsukuba.
Tishchenko, P., Hensen, C., Wallmann, K., Wong, C.S., 2005. Calculation of the stability and solubility of methane hydrate in seawater. Chemical Geology 219, 37–52.
Turner, D.J., Cherry, R.S., Sloan, E.D., 2005. Sensitivity of methane hydrate phase equilibria to sediment pore size. Fluid Phase Equilibria 228–229, 505–510.
Wong, H.K., Lüdmann, T., Baranov, B.V., Karp, B.Y., Konerding, P., Ion, G., 2003. Bottom current-controlled sedimentation and mass wasting in the northwestern Sea of Okhotsk. Marine Geology 201, 287–305.
Worrall, D.M., Kruglyak, V., Kunst, F., Kuznetsov, V., 1996. Tertiary tectonics of the Sea of Okhotsk, Russia: far-field effects of the India-Eurasia collision. Tectonics 15, 813–826.
Xu, W., Ruppel, C., 1999. Predicting the occurrence, distribution, and evolution of methane gas hydrate in porous marine sediments. Journal of Geophysical Research 104, 5081–5095.
Yamano, M., Uyeda, S., Aoki, Y., Shipley, T.H., 1982. Estimates of heat flow derived from gas hydrates. Geology 10, 339–343.
Zonenshayn, L.P., Murdmaa, I.O., Baranov, V., Kuznetsov, A.P., Kuzmin, M.I., Avdeiko, G.P., Stunzhas, P.A., Lukashin, V.N., Barash, M.S., Valyashko, G.M., Dyomina, L.L., 1987. An underwater gas source in the Sea of Okhotsk. Oceanography 27 (5), 598–602.